Vertically averaged approaches for CO_2 migration with solubility trapping

S. E. Gasda,[1] J. M. Nordbotten,[2,3] and M. A. Celia[3]

Received 7 January 2010; revised 19 February 2011; accepted 9 March 2011; published 20 May 2011.

[1] The long-term storage security of injected carbon dioxide (CO_2) is an essential component of geological carbon sequestration operations. In the postinjection phase, the mobile CO_2 plume migrates in large part because of buoyancy forces, following the natural topography of the geological formation. The primary trapping mechanisms are capillary and solubility trapping, which evolve over hundreds to thousands of years and can immobilize a significant portion of the mobile CO_2 plume. However, both the migration and trapping processes are inherently complex, spanning multiple spatial and temporal scales. Using an appropriate model that can capture both large- and small-scale effects is essential for understanding the role of these processes on the long-term storage security of CO_2 sequestration operations. Traditional numerical models quickly become prohibitively expensive for the type of large-scale, long-term modeling that is necessary for characterizing the migration and immobilization of CO_2 during the postinjection period. We present an alternative modeling option that combines vertically integrated governing equations with an upscaled representation of the dissolution-convection process. With this approach, we demonstrate the effect of different modeling choices for typical large-scale geological systems and show that practical calculations can be performed at the temporal and spatial scales of interest.

Citation: Gasda, S. E., J. M. Nordbotten, and M. A. Celia (2011), Vertically averaged approaches for CO_2 migration with solubility trapping, *Water Resour. Res.*, *47*, W05528, doi:10.1029/2010WR009075.

1. Introduction

[2] Geological carbon sequestration is a promising carbon mitigation strategy that can produce significant cuts in CO_2 emissions and help to stabilize atmospheric concentrations at levels that might avoid catastrophic climate change [*Benson et al.*, 2005; *Holloway*, 2005; *Barker et al.*, 2007; *Pacala and Socolow*, 2004]. The storage security of injected CO_2 is an important factor in the success of this technology, which means ensuring that one of several primary trapping mechanisms is able to minimize unwanted migration of separate phase CO_2 out of the targeted injection zone. During the injection phase or early postinjection phase, storage security depends on a competent, relatively impermeable caprock to prevent vertical migration (structural trapping) [*Benson et al.*, 2005]. Factors that can compromise storage security in this period include leakage pathways that are small compared to the extent of the mobile CO_2 plume and can be either natural, such as faults and fractures, or anthropogenic, such as abandoned oil and gas wells [*Benson et al.*, 2005; *Gasda et al.*, 2004; *Celia and Nordbotten*, 2009].

[3] Assuming short-term escape of CO_2 can be managed by proper site selection or appropriate monitoring and remediation strategies, the focus of storage security then shifts, in the long term, to other trapping mechanisms that evolve more slowly. These longer-term mechanisms lead to increasing storage security over time as the mobile CO_2 plume is trapped either as a residual phase (capillary trapping) or as a dissolved phase (solubility trapping), both of which keep the CO_2 underground over timescales of many hundreds to thousands of years or more [*Benson et al.*, 2005]. One important aspect of solubility trapping is the onset of convective mixing, which has potentially significant implications for the extent to which solubility trapping will effectively immobilize separate phase CO_2 [*Lindeberg and Wessel-Berg*, 1997; *Ennis-King and Paterson*, 2005].

[4] The ability to understand the long-term evolution of convective mixing over large spatial scales in complex geological systems is important for proper site selection and risk management. Analytical and semianalytical methods [e.g., *Huppert and Woods*, 1995; *Lyle et al.*, 2005; *Nordbotten and Celia*, 2006; *Hesse et al.*, 2008; *Juanes et al.*, 2010; *Neufeld and Huppert*, 2009] are limited in the complexity of processes and systems that can be modeled. Similarly, high-resolution numerical approaches [e.g., *Lindeberg et al.*, 2003; *Riaz et al.*, 2006; *Farajzadeh et al.*, 2007; *Pruess*, 2008] are limited by computational constraints, which limit the domain size or the number of grid blocks. For convective mixing, very fine grid blocks may be required to resolve the critical wavelength of instability (0.1–1 m for typical systems) to properly capture the onset of convective mixing. Given these drawbacks, it is extremely difficult, if not impossible, to model CO_2 dissolution and convection at the length scales and timescales appropriate for evaluating long-

[1]Environmental Sciences and Engineering, University of North Carolina at Chapel Hill, Chapel Hill, North Carolina, USA.
[2]Department of Mathematics, University of Bergen, Bergen, Norway.
[3]Department of Civil and Environmental Engineering, Princeton University, Princeton, New Jersey, USA.

Copyright 2011 by the American Geophysical Union.
0043-1397/11/2010WR009075

term storage security. Therefore, fast models are required that can capture the essential physics of the postinjection period without excessive computational expense. These types of models may then be used within a Monte Carlo type of approach to understand and assess the risks of long-term storage security for real systems.

[5] An important conclusion from highly resolved computational studies of the dissolution-convection process over relatively small domains is that the onset time of instability is relatively short for typical systems, on the order of 1 year. Additionally, once convective mixing has been induced by the development of convective fingers, the largest fingers progress downward at a constant rate ranging from 0.01 to 1 m yr^{-1} [*Riaz et al.*, 2006], which implies a constant mass transfer rate when scaled by the density of brine with dissolved CO_2. The rate of dissolution due to convective mixing is strongly dependent on the average permeability of the system, including the existence of vertical layering or anisotropy, which can retard the convective mixing process. However, with the results of these studies and an appropriate expression for the effective vertical permeability the complex dissolution-convection process may be modeled as a sub-grid-block-scale process and incorporated into relatively coarse-grid numerical methods.

[6] In this paper, we extend our previous work on vertically integrated numerical models of CO_2 injection to include the effect of dissolution and convective mixing. We will briefly review our overall numerical model, which has been presented in greater detail by *Gasda et al.* [2009], and introduce a novel upscaled approach to convection-enhanced dissolution that is now included in the model. This approach does not explicitly resolve the onset of instability and dissolution finger evolution but, instead, captures the first-order effects of convective mixing through an upscaled mass transfer equation. The result is a modeling tool that captures the dominant physical features of CO_2 migration along varying topography and complex geology in two lateral dimensions, including the primary trapping mechanisms, capillary and solubility trapping, that occur over thousand year timescales.

[7] We use this approach to evaluate the effect of solubility trapping, driven by convective mixing, which may be an important factor in long-term storage security of CO_2 injection operations. We start with an idealized problem that is the subject of a recent benchmark study on long-term CO_2 migration. This problem demonstrates the model concept and the effect of solubility trapping over thousands of years in a simple sloping aquifer system. We then apply the model to a more complex, heterogeneous, and very large geological system that is a prospective site for CO_2 injection under the North Sea. Although to date there are no data for validation of the model results, we are able to show the effect of heterogeneity and structural complexity on long-term, large-scale CO_2 migration in a real system. Overall, this demonstrates the applicability of vertically integrated models to a real field site where full-physics models cannot be run because of computational limitations.

2. Description of the Physical and Mathematical Model

[8] We model flow in a system consisting of two fluid phases, the CO_2 phase and the brine phase. We also consider CO_2 dissolution into the brine and subsequent transport of dissolved CO_2 within the brine phase. Our starting point in this model development is the vertical integration of the governing three-dimensional equations, including assumptions that will be described herein. It should be noted that vertical integration does not inherently require any assumptions about the system, but we take advantage of certain dominant physical characteristics of the CO_2-brine system to make certain simplifications.

[9] One important assumption is that the two fluid phases have a significant density difference such that the fluids segregate because of gravity, with the lighter CO_2 phase overlying the denser brine phase. This assumption is usually appropriate because the relative timescale of gravity segregation is fast compared to that of overall horizontal flow for typical CO_2-brine systems [*Yortsos*, 1995]. We also consider the system to be in vertical equilibrium (VE) and invoke the Dupuit assumption. Gravity segregation is one category of the general class of VE problems [*Yortsos*, 1995]. Inherent in the concept of VE is that each of the different macroscopic regions is vertically distributed in the aquifer in a well-defined way. In other words, the vertical pressure distribution is easily obtained from the vertical distribution of fluids and components dissolved in those fluids. Also, the vertical distribution of saturations of each phase can be defined unambiguously from the vertically averaged saturation. Vertical equilibrium is typically a valid assumption when the relative length scales are such that the horizontal dimension is much larger than the vertical one [*Lake*, 1989; *Yortsos*, 1995]. The commonly invoked assumption of a sharp interface between the two fluids is not a requirement in order to assume vertical equilibrium.

[10] Under the preceding conditions, the governing equations may be vertically integrated in a straightforward manner. The reader is referred to a rich body of literature on this subject of gravity-segregated flows both with and without a sharp interface assumption [*Dietz*, 1953; *Coats et al.*, 1971; *Lake*, 1989; *Yortsos*, 1995; *Huppert and Woods*, 1995; *Nordbotten and Celia*, 2009; *Dentz and Tartakovsky*, 2009a; *Gasda et al.*, 2009].

[11] In this work, we derive the model equations under the sharp interface assumption, where the local capillary transition zone is small compared to the height of the aquifer. This technique is commonly used, for example, in groundwater aquifer models to describe the location of the water table, leading to the classical porous media equation [*Bear*, 1972; *Freeze and Cherry*, 1979]. Again, we emphasize that this assumption is not an absolute criterion to develop a model for vertically averaged flow, and a similar derivation could be performed to include a capillary transition zone [*Lake*, 1989; *Nordbotten and Dahle*, 2011]. The implications of the sharp interface assumption are discussed in section 4.

[12] In addition, we make a simplifying assumption that the fluid properties of both CO_2 and brine are constant. This assumption is appropriate for brine since it is largely an incompressible fluid. With regard to CO_2, more caution should be taken when applying this simplification. In general, CO_2 density and viscosity depend on the depth of the formation and existing geothermal gradients. In typical sedimentary basins, CO_2 properties do not vary significantly horizontally within formations that are deeper than 1000 m [*Bachu*, 2002]. Large pressure increases may occur during

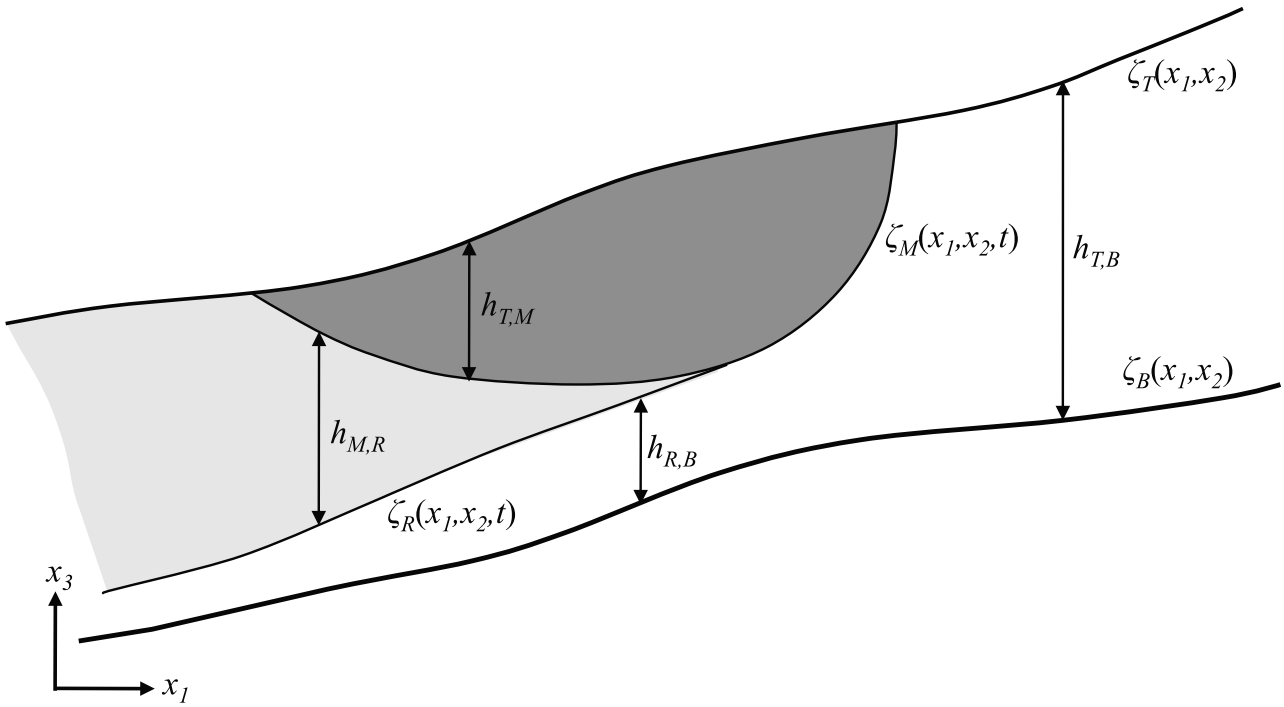

Figure 1. Schematic of the CO_2-brine sharp interface system. The relevant interfaces are the top and bottom surfaces of the formation, $\zeta_T(x_1, x_2)$ and $\zeta_B(x_1, x_2)$, and the interfaces bounding the macroscopic regions of mobile and residual phase CO_2, $\zeta_M(x_1, x_2, t)$ and $\zeta_R(x_1, x_2, t)$. Also given is the thickness h of each macroscopic region of interest.

CO_2 injection, increasing CO_2 density by 100 kg m^{-3} near the wellbore. However, we focus on the postinjection time period in this paper, when pressure due to injection has dissipated and CO_2 migration is governed by buoyancy forces only. Additionally, we should point out that in the model formulation, the overall framework allows for horizontal changes in fluid properties. This would require a nonlinear feedback from the equations of state for CO_2 and brine, but we did not implement this for the examples presented in this study.

[13] This work falls into a robust area of research concerning the application of sharp interface models to CO_2-brine systems. Analytical, semianalytical, and numerical solutions to the sharp interface model have consistently shown relatively good agreement with numerical solutions to the nonaveraged equations for many systems [*Nordbotten and Celia*, 2006; *Class et al.*, 2009] as well as with experimental data [*Huppert and Woods*, 1995; *Lyle et al.*, 2005; *Vella and Huppert*, 2006; *Neufeld and Huppert*, 2009]. There are instances where the application of the sharp interface model has been shown to be inappropriate for certain systems [*Lu et al.*, 2009]. With any model, caution should be taken to apply the model only where the underlying assumptions are valid [*Dentz and Tartakovsky*, 2009b]. For this type of model, the underlying assumptions are most appropriate for studies of long-term CO_2 migration with relative small capillary zones.

[14] We build upon this class of models by adding a solubility-trapping component to account for dissolution due to diffusion- and convection-controlled processes. This model without solubility trapping [*Gasda et al.*, 2009] was previously demonstrated to compare well with commercial and academic full-physics simulators for both idealized systems and general geological systems [*Class et al.*, 2009]. The addition of a long-term dissolution and convective-mixing component to this model does not change the underlying validity of the sharp interface model for systems that exhibit predominantly horizontal flow and small capillary transition zones. We discuss the implications of assumptions made in developing this model at the end of the model presentation.

2.1. System Description

[15] We first present the system description of macroscopic fluid regions and the respective macroscopic interfaces, which includes characterization of the vertical fluid distribution. Next, we develop the set of equations for a vertically integrated model for flow of the CO_2 and brine fluid phases, with special attention paid to dissolution of the CO_2 component into the brine phase. Finally, we describe the method for solving these equations within a numerical framework.

2.1.1. Description of Macroscopic Interfaces

[16] The first step in the model development is the definition of the fluid regions to be modeled, with their respective macroscopic interfaces. The system, shown in Figure 1, is composed of an aquifer, or formation, with top and bottom surfaces $\zeta_T(x_1, x_2)$ and $\zeta_B(x_1, x_2)$ that are well-defined functions in space. In a three-dimensional coordinate system defined by orthogonal unit vectors ($\mathbf{e}_1$, $\mathbf{e}_2$, and $\mathbf{e}_3$) rotated so that the $\mathbf{e}_1$ and $\mathbf{e}_2$ vectors are oriented parallel to the bedding plane, one may interpret these ζ functions as defining the location of the interface in terms of the vertical

coordinate x_3 perpendicular to x_1 and x_2. Within this aquifer, we consider each mobile fluid phase, supercritical CO_2 and brine, to occupy distinct vertical regions, which are also depicted schematically in Figure 1. The bottom macroscopic interface of the mobile CO_2 regions is defined as $\zeta_M(x_1, x_2, t)$.

[17] Because of vertical equilibrium, there is a well-defined transition zone between the two phases controlled by capillary forces. When the transition zone is very small relative to the thickness of the formation, we can neglect the transition zone and model it with a sharp interface. This assumption is employed in this model. Note that in the case where the transition zone is large, we may still define the lower bound of the mobile CO_2 phase as a macroscale interface. The reader is referred to *Nordbotten and Dahle* [2011] for a detailed description of a vertically averaged model for large capillary transition zones. In either case, the vertical pressure distribution is well defined, and the capillary pressure at the macroscopic interface between the mobile CO_2 and brine is the capillary entry pressure in either the drainage or imbibition process.

[18] We also consider other macroscopic regions of fluid distributions, which are also shown in Figure 1. We define a region of residual CO_2 to include all of the CO_2 that is trapped by local capillary forces when the mobile CO_2 interface recedes and brine imbibes into the pore space. Although the residual phase is composed of many small-scale disconnected regions, we will consider as a whole the region that is bounded by a lower macroscale interface $\zeta_R(x_1, x_2, t)$.

[19] We may wish to consider additional macroscale interfaces, such as the separation of the region of mobile CO_2 that contains dissolved water from the dry CO_2 region, but for this study, we will limit our discussion to the three regions of fluids, mobile CO_2, brine phase with residual CO_2, and brine phase without residual CO_2, all of which are distributed vertically within the aquifer. In general, the interfaces must satisfy the criteria that $\zeta_T \geq \zeta_M \geq \zeta_R \geq \zeta_B$.

[20] Within each region, there exist well-defined phase saturations. It is common in sharp interface models to assume that the vertical distribution of fluid properties is constant within each region for a given horizontal (x_1, x_2) location. This means that within the region occupied by mobile or residual CO_2, the density, viscosity, and saturation values are constant. This assumption implies two things; the first is that the CO_2 and brine equations of state are incompressible and thus not a function of pressure and temperature. This constraint is generally valid for brine but may limit the applicability for CO_2 in regions of high gas compressibility. Second, for the sharp interface case, the saturations of CO_2 in the residual region and brine in the mobile CO_2 region are both at their irreducible saturations, $s_{c,r}$ and $s_{b,r}$, respectively. We can summarize the distribution of CO_2 saturation, s_c, in the vertical direction as follows:

$$s_c = \begin{cases} 0 & \text{if} \quad \zeta_B \leq x_3 < \zeta_R, \\ s_{c,r} & \text{if} \quad \zeta_R \leq x_3 < \zeta_M, \\ 1 - s_{b,r} & \text{if} \quad \zeta_M \leq x_3 \leq \zeta_T. \end{cases} \tag{1}$$

In addition, we assume that the porous media properties in the vertical direction are homogeneous. However, all properties may vary as a function of the horizontal direction. The assumption of a constant fluid saturation within macroscopic regions can be easily relaxed if one chooses to model a local capillary transition zone or include subscale heterogeneity in the vertical direction.

2.1.2. Representation of Dissolved Components

[21] We now turn our attention to dissolved constituents. In general, we assume that above the ζ_R interface, both phases exist and the fluids are in chemical equilibrium with respect to dissolved components. This implies that the residual brine above ζ_M and the brine within the residual CO_2 region is saturated with CO_2. Similarly, mobile CO_2 and residual CO_2 are at equilibrium with respect to dissolved water. We do not consider a drying front within the mobile CO_2 region in this work.

[22] The notation employed here for the mass fraction of component α in phase β at equilibrium is $m_\beta^{\alpha,\mathrm{eq}}$. The convention used for variables such as mass, density, and mass fraction is that superscripts refer to components and subscripts refer to phases. For phase density, we refer to the density of a pure phase with only a single component as $\rho_\beta^{\mathrm{pure}}$, while the density of a phase with more than one component is $\rho_\beta^{\mathrm{mix}}$. Therefore, to determine the mass of dissolved CO_2 in the brine phase above the ζ_R interface, the volume of the brine phase with two components is scaled by the quantity $m_b^{c,\mathrm{eq}}\rho_b^{\mathrm{mix}}$ (here we have assumed that the dependence of phase density on dissolved mass fraction is linear, which is reasonable considering that CO_2 is only slightly miscible in water).

[23] In addition to the equilibrium dissolution processes, CO_2 may dissolve into the brine phase across the ζ_R interface. This mass transfer is a transient process that is driven in the long term by convective mixing. This process can be described macroscopically by a growing vertical region of CO_2-saturated brine below the ζ_R interface. This region is parameterized by $\omega(x_1, x_2, t)$, which can be defined as the vertical fraction of the brine region $(\zeta_R - \zeta_B)$ that is saturated with CO_2. The CO_2 dissolved mass in the brine region defined by $(\zeta_R - \zeta_B)$ can be found by scaling ω by the solubility limit $m_b^{c,\mathrm{eq}}$, the density of CO_2-saturated brine ρ_b^{mix}, and the porosity ϕ of the brine region: $\phi\rho_b^{\mathrm{mix}}m_b^{c,\mathrm{eq}}\omega(\zeta_R - \zeta_B)$.

[24] As the value of ω increases, mass conservation dictates that the regions of residual and/or mobile CO_2 must shrink. In this work, we assume that all dissolved CO_2 comes from the residual region of CO_2; as such, the ζ_R interface will move up as ω increases. Because the macroscopic regions are constrained, this has implications for the mobile CO_2 region when $\zeta_M = \zeta_R$ that are discussed in section 2.2.4.

2.1.3. Summary

[25] In summary, the above description of macroscopic interfaces and dissolved CO_2 mass fraction is developed under assumptions of vertical equilibrium, gravity segregation, negligible capillary pressure between CO_2 and brine (sharp interface assumption), and constant fluid saturation and density within each macroscopic region. In the mobile and residual CO_2 regions, where two fluids are present, the saturation of the mobile fluid is such that the trapped phase is at residual saturation. Additional assumptions related to dissolved constituents include equilibrium in the mobile and residual CO_2 regions.

[26] This lays the foundation for how fluids and dissolved components are distributed vertically, which then determines the static vertical pressure distribution. Our objective is to model the evolution of these macroscopic regions, which are

constrained by conservation of mass for CO_2 and brine. In addition, the mass transfer of CO_2 from separate phase to dissolved CO_2 adds a constraint on the system. In section 2.2, we present a consistent mathematical formulation for the evolution of macroscopic interfaces with dissolved CO_2.

2.2. Formulation of Flow and Transport Equations

2.2.1. Mass Balance

[27] We consider the conservation of mass for the two components in the system, CO_2 and brine. The mass of each component α, with $\alpha = c, b$, consists of the sum of mass of α contained in each fluid phase β, for $\beta = c, b$. As described, the fluid phases are divided into separate regions that can be described by their thickness h (e.g., $h_{T,M} \equiv \zeta_T - \zeta_M$). As we noted in section 2.1.1 and equation (1), we assume that the vertical saturation distribution is constant within each region. This also implies that the fluid properties are constant within each vertical region.

[28] We can write the equation for the total mass of brine as the sum of residual brine in the mobile CO_2 region, the brine phase in the residual CO_2 region, and the brine phase in the bottommost region, both with and without dissolved CO_2. Also included in the total brine component mass is the dissolved water in the mobile CO_2 and residual CO_2 regions. We represent these masses as

$$\begin{aligned} M^b = {} & \phi\rho_b^{\text{pure}}(1-\omega)h_{R,B} + \phi\rho_b^{\text{mix}} m_b^{b,\text{eq}} \\ & \cdot \left[\omega h_{R,B} + \left(1 - s_{c,r}\right)h_{M,R} + s_{b,r}h_{T,M}\right] \\ & + \phi\rho_c^{\text{mix}} m_c^{b,\text{eq}}\left[s_{c,r}h_{M,R} + \left(1 - s_{b,r}\right)h_{T,M}\right], \end{aligned} \tag{2a}$$

while total mass of CO_2 is given by

$$\begin{aligned} M^c = {} & \phi\rho_b^{\text{mix}} m_b^{c,\text{eq}}\left[\omega h_{R,B} + \left(1 - s_{c,r}\right)h_{M,R} + s_{b,r}h_{T,M}\right] \\ & + \phi\rho_c^{\text{mix}} m_c^{c,\text{eq}}\left[s_{c,r}h_{M,R} + \left(1 - s_{b,r}\right)h_{T,M}\right]. \end{aligned} \tag{2b}$$

The conservation of total component mass can be written as

$$\frac{\partial M^\alpha}{\partial t} + \nabla \cdot \mathbf{F}^\alpha = 0, \qquad \alpha = c, b, \tag{3}$$

where $\mathbf{F}^\alpha$ is the total flux of component α transported within each of two fluid phases. Let the local volumetric flux of each of the fluid phases be represented by $\mathbf{u}_c(x_1, x_2, x_3, t)$ and $\mathbf{u}_b(x_1, x_2, x_3, t)$. The total component flux $\mathbf{F}^\alpha$ can be obtained by integration of the appropriate local-scale fluid fluxes scaled by the fluid density and mass fraction of the component in that fluid,

$$\mathbf{F}^\alpha = \sum_\beta \int_{\zeta_B}^{\zeta_T} \mathbf{u}_\beta \rho_\beta m_\beta^\alpha \, dx_3. \tag{4}$$

2.2.2. Pressure and Fluid Fluxes

[29] To obtain a vertical distribution of fluxes, we must first describe the vertical pressure distribution for a VE system. In a fluid-static system, the vertical distribution of pressure $p(x_3)$ is simply a function of the vertical fluid density profile, defined generally as $\rho(x_3)$. The pressure can be obtained by the integration of the density profile along x_3, assuming the gravitational vector $\mathbf{g}$ is aligned with the vertical coordinate. If we define a reference pressure datum ζ_P, we obtain the following expression for pressure:

$$p(x_3) - p(\zeta_P) = \mathbf{e}_3 \cdot \mathbf{g} \int_{\zeta_P}^{x_3} \rho(x_3') \, dx_3'. \tag{5}$$

The elevation of ζ_P is typically either set equal to a constant elevation or referenced to some combination of the top and bottom boundaries of the formation. Given the definition in equation (5) and the description of macroscopic fluid regions in section 2.1.1, the vertical distribution of pressure for this system can be written as

$$p(x_3) = \begin{cases} p(\zeta_P) + \mathbf{e}_3 \cdot \mathbf{g}\left[\rho_b^{\text{pure}}(1-\omega) + \rho_b^{\text{mix}}\omega\right](x_3 - \zeta_P) & \text{if} \quad \zeta_B \le x_3 \le \zeta_R, \\ p(\zeta_R) + \mathbf{e}_3 \cdot \mathbf{g}\rho_b^{\text{mix}}(x_3 - \zeta_R) & \text{if} \quad \zeta_R < x_3 \le \zeta_M, \\ p(\zeta_M) + \mathbf{e}_3 \cdot \mathbf{g}\rho_c(x_3 - \zeta_M) & \text{if} \quad \zeta_M < x_3 \le \zeta_T. \end{cases} \tag{6}$$

Equation (6) is formulated under the assumption that $\zeta_P \le \zeta_B \le \zeta_R \le \zeta_M \le \zeta_T$.

[30] As a result of the Dupuit assumption, the pressure gradient in the $\mathbf{e}_1$ and $\mathbf{e}_2$ directions is independent of the x_3 coordinate. We define the fluid mobility for each phase β as a function of relative permeability and fluid viscosity, $\lambda_\beta(s_c) = k_{r,\beta}(s_c)/\mu_\beta$. Using capital $P = p(\zeta_P)$, we can now use Darcy's law to express the phase fluxes that enter into equation (4). For the brine flux $\mathbf{u}_b$,

$$\begin{aligned} \mathbf{u}_{b,B,R} & \equiv \mathbf{u}_b(\zeta_B \le x_3 \le \zeta_R) \\ & = -k\lambda_b(0)\nabla\left\{P - \mathbf{e}_3 \cdot \mathbf{g}\left[\rho_b^{\text{pure}}(1-\omega) + \rho_b^{\text{mix}}\omega\right]\zeta_P\right\}, \\ \mathbf{u}_{b,R,M} & \equiv \mathbf{u}_b(\zeta_R \le x_3 \le \zeta_M) = -k\lambda_b\left(s_{c,r}\right)\nabla\left\{P + \mathbf{e}_3 \cdot \mathbf{g}\left[\rho_b^{\text{pure}}(1-\omega)\right.\right. \\ & \qquad \left.\left. + \rho_b^{\text{mix}}\omega\right](\zeta_R - \zeta_P) - \mathbf{e}_3 \cdot \mathbf{g}\rho_b^{\text{mix}}\zeta_R\right\}, \\ \mathbf{u}_{b,M,T} & \equiv \mathbf{u}_b(\zeta_M \le x_3 \le \zeta_T) = 0, \end{aligned} \tag{7}$$

where the brine is at residual saturation and thus immobile in the mobile CO_2 region. Similarly, CO_2 is not mobile in regions where the CO_2 is not present or is at residual, so $\mathbf{u}_{c,B,R} = \mathbf{u}_{b,R,M} = 0$. Therefore, the CO_2 phase flux in the mobile region $\mathbf{u}_{c,M,T}$ is defined as

$$\begin{aligned} \mathbf{u}_{c,M,T} \equiv {} & \mathbf{u}_c(\zeta_M \le x_3 \le \zeta_T) = -k\lambda_c\left(1 - s_{b,r}\right) \\ & \cdot \nabla\left\{P + \mathbf{e}_3 \cdot \mathbf{g}\left[\rho_b^{\text{pure}}(1-\omega) + \rho_b^{\text{mix}}\omega\right](\zeta_R - \zeta_P)\right. \\ & \left. + \mathbf{e}_3 \cdot \mathbf{g}\rho_b^{\text{mix}}(\zeta_M - \zeta_R) - \mathbf{e}_3 \cdot \mathbf{g}\rho_c\zeta_M\right\}. \end{aligned} \tag{8}$$

[31] With the above definitions of fluid fluxes, the integral in equation (4) can be evaluated. In the case of vertical permeability heterogeneity, the integral must be evaluated region by region in a piecewise manner along x_3. In the case of homogeneous permeability in the vertical, the integral reduces to a simple scaling of the fluxes by the height of each macroscopic region.

[32] Equations (1)–(8) provide two mass conservation equations and corresponding fluxes. The unknowns we wish

to solve for are the interfaces ζ_M and ζ_R, the thickness of brine saturated with dissolved CO_2 ω, and pressure P. With these variables, all other variables can be reconstructed for the system. The interface and mass fraction variables are constrained by the problem definition described in section 2.1.1; however, additional equations are required to close the system. We achieve this by introducing two equations for the mobile CO_2 interface and for the transport of total dissolved CO_2.

2.2.3. Dissolution and Component Transport

[33] Dissolution of CO_2 into the brine phase occurs wherever the CO_2 fluid phase is in contact with the resident brine. Dissolution across the microscale interface leads to equilibrium concentration in the vicinity of these interfaces at the local scale. Given the usual distribution of residual fluid phases, it is reasonable to assume that the residual brine phase (behind the advancing CO_2 front) would become saturated with dissolved CO_2 relatively quickly. Similarly, the brine phase that is imbibing into the pore spaces containing residual CO_2 would also reach equilibrium in a short amount of time. Therefore, we model these regions using equilibrium partitioning. Note that the amount of dissolved CO_2 in these two regions is relatively small compared to the total amount of mobile CO_2.

[34] CO_2 dissolution has a secondary effect on the system, whereby the region of brine that contains dissolved CO_2 is denser than "pure" brine (brine with no dissolved CO_2). Because the CO_2-saturated brine phase overlies the pure brine phase, the system is inherently unstable, and the saturated brine will sink toward the bottom of the aquifer and induce convective mixing within the system. The onset of convection enhances CO_2 dissolution at the macroscopic CO_2-brine interface beyond a diffusion-controlled process because pure brine will be brought upward as the denser saturated brine sinks. This system has been studied extensively by others [*Ennis-King and Paterson*, 2005; *Lindeberg et al.*, 2003; *Riaz et al.*, 2006; *Farajzadeh et al.*, 2007; *Pruess*, 2008], and it can be concluded from this body of work that the onset time of instability is relatively short for typical systems, on the order of 1 year. Furthermore, it has been shown that once the instability occurs, the effective total mass transfer rate is constant in time. The rate of dissolution due to convective mixing is controlled by the Rayleigh number and is most sensitive to the permeability of the aquifer system and the value of the diffusion coefficient.

[35] We consider mass transfer of CO_2 into the brine phase due to convective mixing to be parameterized by ω, which is the average mass fraction of dissolved CO_2 in the region bounded by ζ_R and ζ_B. We also consider the onset of convective mixing to be instantaneous and the upscaled dissolution rate due to convective mixing C_{diss} to be constant in time and constrained by ω and ζ_R. The value of C_{diss} may vary in space because of heterogeneous permeability. In this paper, we do not consider the evaporation of water into the CO_2 phase or other dissolved components in the brine phase, such as salts.

[36] The mass transfer model may be written by first considering the total mass of dissolved CO_2,

$$M_b^c = \phi \rho_b^{\text{mix}} m_b^{c,\text{eq}} \left[\omega h_{R,B} + \left(1 - s_{c,r}\right) h_{M,R} + s_{b,r} h_{T,M} \right], \quad (9)$$

which takes into account CO_2 dissolved in three regions: (1) in the residual brine behind the invading CO_2 front; (2) in brine imbibing into pore space containing residual CO_2; and (3) in the fraction of brine below the residual CO_2 region that is saturated with dissolved CO_2.

[37] The total mass of dissolved CO_2 is a conserved quantity and evolves according to the following transport equation:

$$\frac{\partial M_b^c}{\partial t} + \nabla \cdot \int_{\zeta_B}^{\zeta_T} \mathbf{u}_b \rho_b m_b^c \, dx_3 = C_{\text{diss}}(\omega, \zeta_R), \quad (10)$$

where the right side represents the transient mass transfer due to convective mixing, which is constrained by $0 \le \omega \le 1$. The constrained nature of equation (10) can be seen most easily by first substituting equation (9) into equation (10) and rearranging so that it is written as an expression for the time derivative of ω. In doing so, we define the integral-differential operator $\mathcal{D}_1$ as

$$\mathcal{D}_1 \equiv \frac{C_{\text{diss}}(\omega, \zeta_R) - \nabla \cdot \int_{\zeta_B}^{\zeta_T} \mathbf{u}_b \rho_b m_b^c \, dx_3}{\phi \rho_b^{\text{mix}} m_b^{c,\text{eq}} h_{R,B}} - \frac{\omega}{h_{R,B}} \frac{\partial h_{R,B}}{\partial t} - \frac{1}{h_{R,B}} \frac{\partial}{\partial t} \left[\left(1 - s_{c,r}\right) h_{M,R} + s_{b,r} h_{T,M} \right], \quad (11)$$

which shows the time rate of change of the dependence of ω on the collection of processes that increase or decrease total dissolved CO_2. To capture the upper and lower limits on dissolution, we have the following constraints:

$$\frac{\partial \omega}{\partial t} = \begin{cases} \max(0, \mathcal{D}_1) & \text{if} \quad \omega = 0, \\ \min(0, \mathcal{D}_1) & \text{if} \quad \omega = 1, \\ \mathcal{D}_1 & \text{otherwise.} \end{cases} \quad (12)$$

[38] Let us consider the first constraint, which states that if $\omega = 0$, then ω may increase only if $\mathcal{D}_1$ is greater than zero. If we consider a simple example of this scenario at the leading edge of the advancing CO_2 front, when $h_{M,R} = 0$, the only terms to survive are the first and last terms in equation (11). This implies that ω will increase only if the rate of the advancing front is slower than C_{diss}. If the velocity of the front is faster than the rate of mass transfer, then dissolved CO_2 is only created in the residual brine phase that forms behind the advancing front.

[39] The second constraint applies to scenarios when $\omega = 1$, in which case, ω can only decrease or remain unchanged. Let us take another simple example of this case at the location where the mobile CO_2 region has completely receded ($h_{T,M} = 0$). In this case, the transport of dissolved CO_2 becomes an important factor (the divergence operator), which can reduce the average concentration if there is an upwelling of pure brine at that location. However, this process competes with mass transfer of CO_2 from the residual region. If these processes balance or if C_{diss} is greater than the loss of dissolved CO_2 due to transport, then ω remains equal to unity; otherwise, ω will decrease.

2.2.4. Solution for Mobile and Residual CO_2 Interfaces

[40] We wish to describe the evolution of the interfaces that bound the mobile and residual CO_2 regions. This equation will close the system of equations. To begin, we consider the ζ_R interface, which we recall is the lower bound of the residual CO_2 region. In the absence of dissolution, $\zeta_R(t)$ would be modeled simply as the lowest vertical extent of the mobile interface ζ_M over all time, which can be

written as $\zeta_R(t) = \min_{t' \leq t} \zeta_M(t')$. The effect of dissolution gives a more complicated formulation of the ζ_R interface evolution. First, we account for dissolution due to convective mixing into the macroscopic region below ζ_R by assuming that the source of dissolved CO_2 is from the residual CO_2 region only. For the model to be consistent with this idea, the ζ_R interface will recede as dissolution occurs. When $\zeta_R < \zeta_M$, this is a straightforward mass balance. However, when $\zeta_R = \zeta_M$, then the evolution of the mobile interface must account for the effect of dissolution since in this case $\zeta_M = \zeta_R$.

[41] Given the above discussion, we now consider the mobile CO_2 interface ζ_M, which evolves according to the conservation equation for the mobile CO_2,

$$-\phi\left(1 - s_{c,r} - s_{b,r}\right)\frac{\partial \zeta_M}{\partial t} + \nabla \cdot \int_{\zeta_M}^{\zeta_T} \mathbf{u}_c \, dx_3 = 0. \tag{13}$$

The integrated flux accounts for the fact that CO_2 is only mobile within the region bounded by ζ_T and ζ_M. Equation (13) may be solved in the presence or absence of dissolution. If porosity varies vertically, then ϕ would be calculated as an average porosity over the $h_{T,M}$. To show the effect of the aforementioned constraints on the mobile CO_2 interface, we form an operator $\mathcal{D}_2$ from equation (13),

$$\mathcal{D}_2 \equiv \frac{\nabla \cdot \int_{\zeta_M}^{\zeta_T} \mathbf{u}_c \, \mathrm{d}x_3}{\phi\left(1 - s_{c,r} - s_{b,r}\right)}. \tag{14}$$

The time rate of change of ζ_M is then constrained as follows:

$$\frac{\partial \zeta_M}{\partial t} = \begin{cases} \min(0, \mathcal{D}_2) & \text{if} \quad \zeta_M = \zeta_T, \\ \max\left(\dfrac{\partial \zeta_R}{\partial t}, \mathcal{D}_2\right) & \text{if} \quad \zeta_M = \zeta_R, \\ \mathcal{D}_2 & \text{otherwise.} \end{cases} \tag{15}$$

[42] We observe that the first constraint reflects the case at the leading edge of the advancing CO_2 front, where the brine phase is undergoing primary drainage. In this case, the mobile CO_2 interface will decrease (the height $h_{T,M}$ of the mobile CO_2 region will increase). Because the thicknesses of the mobile and residual regions are initially zero, the maximum value of the ζ_M interface is constrained by the top surface of the formation ζ_T. If the value of $\mathcal{D}_2$ is less than zero in this case, then ζ_M moves downward, and mobile CO_2 appears.

[43] An example of the second constraint is in the advancing mobile CO_2 region, but where mobile CO_2 already exists ($\zeta_M < \zeta_T$). In this case, there is no residual region, but the minimum location of the ζ_M interface is constrained by the location of ζ_R. If dissolution is occurring according to equation (11), then the ζ_R interface recedes because of the mass balance of total CO_2, and the mobile interface must recede also.

2.2.5. Summary

[44] In total, equations (3), (12), and (15) now form a system of partial differential equations governing the evolution of pressure, mobile and residual CO_2 regions, and concentration of dissolved CO_2 in brine. A few aspects of this model should be pointed out. First, there exists some flexibility in the closure equations (12) and (15), and we have chosen a particular model for this formulation. Other formulations of the subscale interface and dissolved component transport are equally favorable options. As one example, we have assumed a uniform distribution of concentration in the brine region $h_{R,B}$, while one could argue that there would be a higher concentration of CO_2 near the top of this region. This would impact the integral terms in equations (10) and (11).

[45] A consequence of introducing the vertical structure of the CO_2 concentration in the brine region is that the coarse-scale equations now inherit the property that makes the fine-scale system unstable: denser brine is above lighter brine. It is therefore expected that integrated models that do not assume uniform distribution of concentration in the brine region may be unstable, particularly if applied to spatial scales where the fine-scale problem develops fingers. A full discussion of these issues go beyond the scope of this paper. However, our current calculations indicate good behavior of the model as currently formulated.

2.3. Implicit Pressure Explicit Saturation Type Solution Strategy

[46] We solve the system of equations in a numerical framework using a standard cell-centered finite difference approximation within an Implicit Pressure Explicit Saturation (IMPES) type solution strategy. This approach allows for flexibility in modeling general geological systems that are heterogeneous and have moderate structural complexity. It should be noted that the primary objective of this paper is the model formulation, and the choice of the numerical solution method is secondary. In fact, any numerical approach can be employed to solve the model equations, and in this study, we choose the IMPES method largely because it is convenient to implement and it performs well in our test simulations.

2.3.1. Pressure Equation

[47] We start by formulating a pressure equation from the mass conservation equations, (3) and (10). We restrict our attention to incompressible systems. This assumption is made solely for the simplicity of numerical implementation and is not inherent in the general model formulation. For an incompressible system, we may consider conservation of volume instead of conservation of mass. We consider three volumes that compose the system of interest, the volume of the CO_2 mixture V_c^{mix}, the volume of the brine mixture V_b^{mix}, and the volume of pure brine V_b^{pure}. The total component masses M^c and M^b can be expressed in terms of these volumes,

$$M^c = \phi \rho_c^{\mathrm{mix}} m_c^{c,\mathrm{eq}} V_c^{\mathrm{mix}} + M_b^c \tag{16}$$

$$M^b = \phi \rho_b^{\mathrm{pure}} V_b^{\mathrm{pure}} + \phi \rho_b^{\mathrm{mix}} m_b^{b,\mathrm{eq}} V_b^{\mathrm{mix}} + \phi \rho_c^{\mathrm{mix}} m_c^{b,\mathrm{eq}} V_c^{\mathrm{mix}}, \tag{17}$$

where the mass of dissolved CO_2 can be expressed as

$$M_b^c = \phi \rho_b^{\mathrm{mix}} m_b^{c,\mathrm{eq}} V_b^{\mathrm{mix}}. \tag{18}$$

[48] Summing over equations (3) and (10) and making the appropriate substitutions from equations (16)–(18), we obtain a pressure equation,

$$\frac{1}{\phi \rho_b^{\mathrm{pure}}} \nabla \cdot \mathbf{F}^b + \left(\frac{1}{\phi \rho_c^{\mathrm{mix}} m_c^{c,\mathrm{eq}}} - \frac{m_c^{b,\mathrm{eq}}}{\phi \rho_b^{\mathrm{pure}} m_c^{c,\mathrm{eq}}}\right) \nabla \cdot \mathbf{F}^c + V_\phi \left(\nabla \cdot \mathbf{F}_b^c\right) = V_\phi C_{\mathrm{diss}}, \tag{19}$$

where V_ϕ is the volume change due to dissolution per unit mass of CO_2 dissolved,

$$V_\phi = \frac{1}{\phi\rho_b^{\mathrm{mix}} m_b^{c,\mathrm{eq}}} - \frac{1}{\phi\rho_c^{\mathrm{mix}} m_c^{c,\mathrm{eq}}} + \frac{m_c^{b,\mathrm{eq}}}{\phi\rho_b^{\mathrm{pure}} m_c^{c,\mathrm{eq}}} - \frac{m_b^{b,\mathrm{eq}}}{\phi\rho_b^{\mathrm{pure}} m_b^{c,\mathrm{eq}}}. \quad (20)$$

Equation (19) contains a divergence of component fluxes, which are functions of the phase fluxes. The right side of the equation accounts for the decrease in volume that occurs when CO_2 is transferred from the mobile or residual state to the dissolved state. The volume change factor V_ϕ is equal to zero for an isovolumetric system.

[49] Equation (19) can be converted to the divergence of phase fluxes through substitution of equation (4),

$$\frac{1}{\phi}\nabla\cdot\left(h_{T,M}\mathbf{u}_{c,M,T} + h_{M,R}\mathbf{u}_{b,R,M} + h_{R,B}\mathbf{u}_{b,B,R}\right) = V_\phi C_{\mathrm{diss}}. \quad (21)$$

Equation (21) is converted to a pressure equation by substitution of the phase flux definitions in (7) and (8). It is then solved implicitly using a standard finite difference approximation with upstream-weighted mobility values within the IMPES framework.

2.3.2. Saturation Solver

[50] For the transport equations, we consider a splitting type approach, evolving ζ_M first, then ζ_R, and, finally, the concentration ω.

[51] To evolve ζ_M, we utilize equation (15), except in the case where $\partial\zeta_M/\partial t = \partial\zeta_R/\partial t$, where we solve for both ζ_M and ζ_R simultaneously using equation (3). After solving for ζ_M explicitly, we solve ζ_R by using the difference between equation (3) and equation (15), which ensures that mass is conserved. Finally, we solve for ω explicitly using equation (12). The time step size for the explicit solve is constrained by a CFL condition on the velocity of the mobile CO_2 interface.

[52] It should be noted that the above solution approach cannot be applied to an isovolumetric system. This is because there is not a one-to-one relationship between masses (M^α and M_b^c) and macroscopic region elevations ($h_{T,M}$, $h_{M,R}$, $h_{R,B}$, and ω) when $V_\phi = 0$. None of the systems we consider are isovolumetric.

3. Model Application

[53] We employ the model described above to evaluate the importance of dissolution and convection over different spatial and temporal scales appropriate for geological carbon sequestration. We begin with a benchmark study proposed by H. K. Dahle et al. (A model-oriented benchmark problem for CO_2 storage, 2009, http://arks.princeton.edu/ark:/88435/dsp01pn89d657g, hereinafter Dahle et al., 2009) that features a relatively simple geological storage problem. This problem is designed to highlight important questions regarding the long-term fate of the injected CO_2 and to assess the impact of different modeling approaches. We evaluate the effect of convection-enhanced dissolution on the eventual immobilization of CO_2 in this simplified system. The second problem is a variation on a previous benchmark problem involving the Johansen formation, a subseabed saline aquifer off the Norwegian coast. This problem has been described in detail elsewhere [*Class et al.*, 2009; *Eigestad et al.*, 2009]. In this paper, we choose to extend the problem to investigate the long-term effects of convection-enhanced dissolution.

3.1. Benchmark Definition

[54] A brief summary of the problem definition is provided, with a more detailed description available from Dahle et al. (2009). The benchmark system is a 50 m thick aquifer that is sloping with a 1% dip and bounded on the top and bottom by impermeable formations. The side boundaries are open to flow along the entire extent of the domain. The injection of CO_2 into this system occurs through a 1 km long horizontal well, oriented perpendicular to the dip direction, at a rate of 1 megaton (Mt) yr^{-1} for 20 years.

[55] The rock properties are homogeneous, with a permeability of 1×10^{-13} m^2 and a porosity of 15%. The fluid properties are chosen to be constant values of 1099 and 733 kg m^{-3} for the density and 0.511 and 0.0611 mPa s for the viscosity of the brine and CO_2 phases, respectively. Hysteresis in the relative permeability function is included for this system. The bounding relative permeability for brine at $s_{c,r} = 0.20$ is $k_{r,b} = 0.32$, while for CO_2 the maximum relative permeability is $k_{r,c} = 0.4$ at $s_{b,r} = 0.20$. A local capillary pressure function is assigned for the benchmark problem, but it is neglected under the assumption of a sharp interface.

3.1.1. Modeling Choices

[56] The benchmark problem is solved under the assumption of line symmetry along the center axis of the domain, parallel to the direction of dip. The width of the CO_2 plume in the transverse direction is assumed to be 1 km, which is equal to the length of the horizontal injection well, which implies no transverse spreading. The injection rate is divided by 1 km to account for the line symmetry. Constant grid spacing of 250 m is employed along the dip direction.

[57] For the simulations that include the dissolution-convection model, we choose the upscaled dissolution rate C_{diss} to be 0.44 kg m^{-2} yr^{-1}, which corresponds to a convective finger speed of 0.13 m yr^{-1} [*Riaz et al.*, 2006]. This choice of dissolution rate is relatively conservative. In addition, the saturated mass fraction of dissolved CO_2 in brine $m_b^{c,\mathrm{eq}}$ is assigned as 2%, which gives an apparent CO_2 density for this system, $\rho_b^{\mathrm{mix}} m_b^{c,\mathrm{eq}} = 22$ kg m^{-3}. The value of $m_b^{c,\mathrm{eq}}$ is low relative to the maximum value of approximately 5% for typical CO_2 sequestration systems [*Benson et al.*, 2005]. However, a lower value reflects the fact that the convective mixing does not lead to full saturation in the brine column beneath the mobile CO_2 phase. This is because the large dissolution fingers, once formed, do not coalesce in the lateral direction but, instead, travel downward relatively independently [*Riaz et al.*, 2006]. Thus, for most systems, the effect of independent fingers leads to an average concentration of dissolved CO_2 over a grid block that is less than the fully saturated concentration.

3.1.2. Benchmark Results

[58] The benchmark results are presented to address the questions posed by the benchmark study (Dahle et al., 2009) and were designed to determine the ultimate fate of the injected plume during the postinjection period. They include three reported measures: (1) the maximum upslope extent of the plume at three specified times, (2) the distribution of

Table 1. Summary of Benchmark Results

C_{diss} (kg m^{-2} yr^{-1})	Years Postinjection	Maximum Upslope Extent (km)	Percent CO_2 Mass		
			Mobile	Residual	Dissolved
0	0	12.6	100	0	–
0	100	13.4	98	2	–
0	22,000	>150	18	82	–
0.44	0	11.1	99	0	1
0.44	100	9.6	94	1	5
0.44	12,000	52.4	0	52	48

CO_2 mass in the mobile, residual, and dissolved states, and (3) the time to complete immobilization of the CO_2 . These data are given in Table 1, and a discussion of the results is provided herein. Only results that invoke line symmetry are presented in this paper, but the reader is referred to J. M. Nordbotten et al. (Computational results for CO_2 migration under a sloping caprock, manuscript in preparation, 2011) for detailed results from other simulations that model the transverse direction.

[59] When the benchmark system is modeled without solubility trapping (Figure 2), the simulation results show the CO_2 plume reaching the domain boundary, 150 km from the point of injection, after 22,000 years, before all the CO_2 is entrapped in the residual phase. At the time the plume reaches the boundary, 82% of the injected mass has been trapped residually. A plot of the distribution of CO_2 mass between the mobile phase and residual phase in Figure 3 shows that there is a high rate of entrapment initially, which gradually slows as the plume travels updip. The sweep efficiency of the plume in the vertical direction decreases as the plume migrates and spreads updip, which accounts for the slow rate of entrapment at late times.

[60] The inclusion of the convection-enhanced dissolution model (Figure 4) leads to significantly different behavior. The CO_2 plume does not travel as far as the case when dissolution effects are not modeled, nor does it remain mobile for as long a time. It is clear from Figure 4 that the plume is immobilized before it travels more than about 50 km updip from the injection well. Complete immobilization occurs within 12,000 years postinjection. Figure 5 shows that the final distribution of total CO_2 mass is almost equally distributed between the residual and dissolved phases. This indicates that solubility trapping and capillary trapping are equally important in this problem. Furthermore, it appears that the rate of capillary trapping does not change significantly when dissolution-convection effects are modeled. This is evident by looking at the same point in time (10,000 years), where there is nearly the same proportion of CO_2 mass in the residual phase when

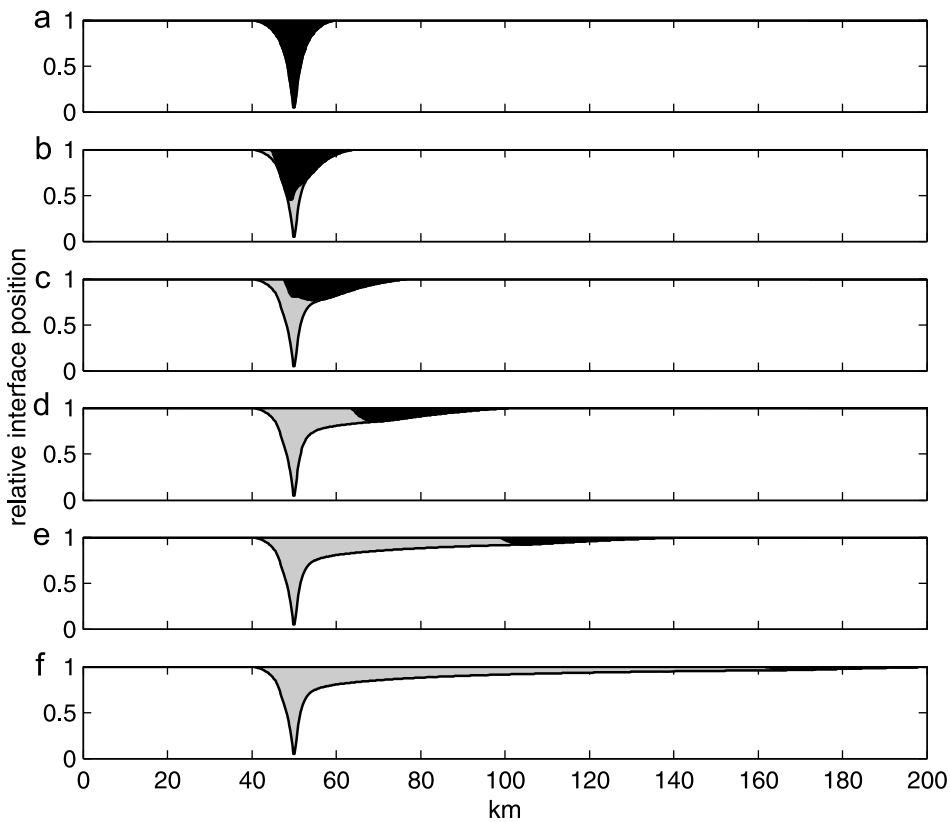

Figure 2. Numerical results of the benchmark problem without dissolution effects. The plots show the evolution of CO_2 in the mobile state (black area) and in the residual state (dark gray area) over time in the postinjection period at the following times: (a) 0 years, (b) 600 years, (c) 2500 years, (d) 6250 years, (e) 12,500 years, and (f) 22,000 years.

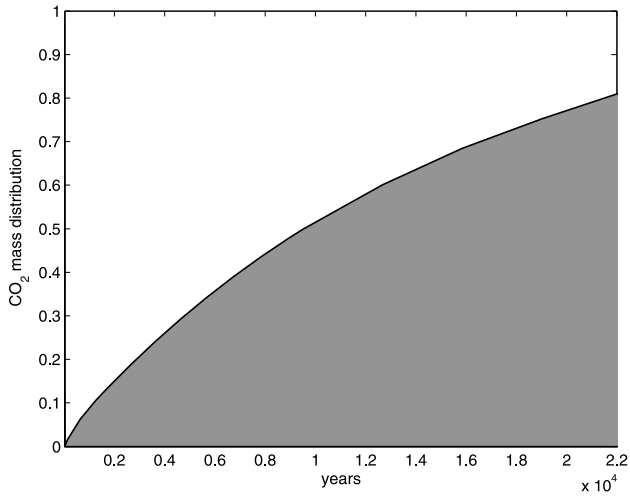

Figure 3. Distribution of CO_2 mass over time for the benchmark problem without dissolution effects. The fraction of total CO_2 mass in the mobile phase is indicated by the white area and that in the residual phase by the dark gray area.

dissolution-convection processes are modeled (45%) as when they are not (49%). Examination of the rate of mass trapped in residual phase in both cases, although not shown here, confirms this observation.

[61] Figure 5 also indicates that the rate of CO_2 mass transfer into the dissolved state is higher in the early post-injection period (<200 years) and gradually slows to a nearly constant rate before mobile CO_2 is depleted. This occurs in part because CO_2 entrapment in the residual phase is also maximum at this time, and therefore, the mass transfer of CO_2 into the brine phase that imbibes into the residual phase region, which we recall is an instantaneous process in this model, leads to a large amount of dissolved CO_2. This dissolution associated with imbibition accounts for nearly all of the dissolved CO_2 at early postinjection time.

[62] It should also be noted in Figure 5 that the slight increase in dissolved CO_2 mass once the mobile CO_2 has been depleted is due to the mass transfer of CO_2 from the residual phase that remains once the mobile CO_2 is completely entrapped. We observe that the residual phase is being dissolved at a much slower rate than the mobile phase CO_2, indicating that this process may be considered a secondary effect that is likely on the same timescale as CO_2 mineralization processes.

[63] The benchmark results can also be analyzed by examining the influence of dissolution-convection effects on the effective rate of migration. In Figure 6, we observe that in the absence of dissolution, the tip velocity is driven only by buoyancy and reaches a relatively constant rate of migration quickly. On the other hand, convection-enhanced dissolution decreases the effective rate of plume migration by approximately 50%. This should not be equated with a

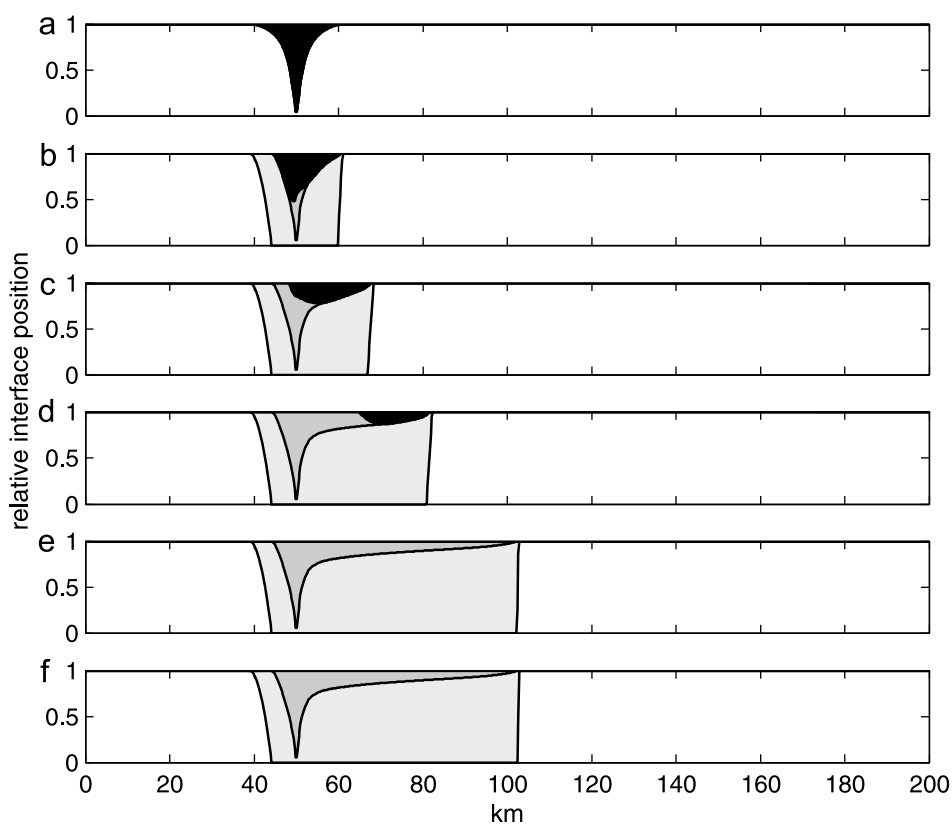

Figure 4. Numerical results of the benchmark problem with dissolution-convection effects included. The plots show the evolution of CO_2 in the mobile state (black area), in the residual state (dark gray area), and in the dissolved state (light gray area) over time in the postinjection period at the following times: (a) 0 years, (b) 600 years, (c) 2500 years, (d) 6250 years, (e) 12,500 years, and (f) 22,000 years.

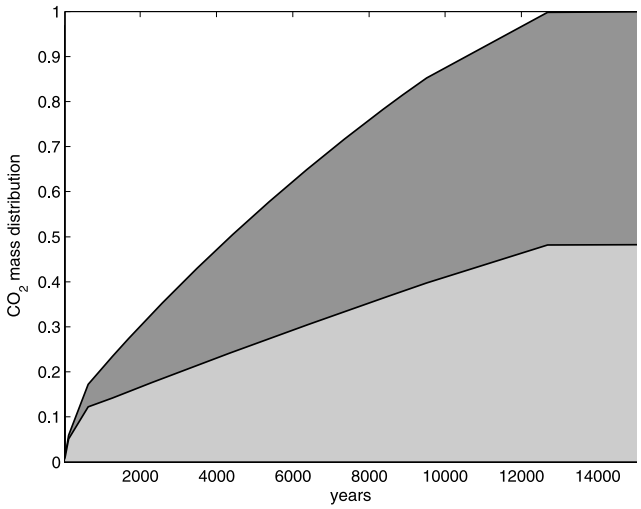

Figure 5. Distribution of CO_2 mass over time for the benchmark problem with dissolution-convection effects included. The fraction of total CO_2 mass in the mobile phase is indicated by the white area, that in the residual phase by the dark gray area, and that in the dissolved phase by the light gray area.

reduction in the buoyancy of the plume, but rather with the similar timescales of buoyancy drive and convection-enhanced dissolution rate, which result in the leading edge of the plume being dissolved almost as fast as it is traveling upslope. This interplay between buoyancy and dissolution is quite evident in the early time behavior of the plume, where the maximum upslope extent of the plume retracts from 11.1 km at the end of injection to 9.6 km 100 years after injection (see Table 1). This effect is entirely due to dissolution immobilizing the CO_2 at a faster rate than the plume can advance due to buoyancy. It should be noted that since this is not a perfectly hyperbolic system, the influence of buoyancy on the tip velocity is less at early times than at later times.

3.2. Full Johansen Results

[64] The vertically averaged model with solubility trapping is applied to a general geological formation to examine the effect of long-term dissolution-convective mixing in a more natural, heterogeneous system. The Johansen formation, located under the North Sea off the coast of Norway, has been identified as a likely candidate to sequester CO_2 emissions from large onshore point sources. The brine-bearing formation has an areal extent of 60 km × 60 km and is characterized by a distinctive fault that not only is sealing but also effectively splits the formation into two parts; the northeast portion has an updip, and the southwest portion has a downdip (Figure 7). The formation is heterogeneous in both porosity and permeability. The heterogeneity field is constructed from depth-correlated values that were derived from core data. The geological and hydrological setting has been described in detail elsewhere [*Eigestad et al.*, 2009], and a portion of the formation has been the subject of a previous benchmark study [*Class et al.*, 2009]. The detailed information in those publications will not be repeated here.

[65] We extend a previous study of CO_2 injection into the Johansen formation [*Gasda et al.*, 2009], where 1 Mt yr^{-1} of CO_2 is injected for a 50 year period. In the original study, residual trapping was the only process modeled during the postinjection period. Fluid properties are constant, and local residual saturations are $s_{c,r} = 0.5$ and $s_{b,r} = 0.2$. The extent of CO_2 trapping over the 100 year postinjection period in that study was found to be over 50% of the total injected mass.

[66] This same system was modeled in an identical manner but with the addition of dissolution-convection effects. The upscaled dissolution rate is assigned as 0.44 kg m^{-2} yr^{-1}, a relatively conservative value, as discussed in section 3.1.1. In Figure 7, we see that the mobile CO_2 interface migrates updip as a contiguous plume within the first 100 years, but then the plume breaks up into smaller plumes as most of the CO_2 mass becomes trapped in the residual or dissolved states. The shape of the region of residually trapped CO_2 follows the general pattern of the mobile plume. Within 2000 years, the thinner portions of the residual region, toward the left and right, are completely dissolved. The region of dissolved CO_2 grows as the mobile CO_2 migrates updip and then is essentially static after 2000 years.

[67] The effect of dissolution leads to nearly complete immobilization within just 2000 years (Figure 8). The amount of mass that exists in the dissolved phase at 2000 years is approximately 53%, with 46% in the residual state. The remaining 1% of CO_2 mass is in the mobile phase, an amount that persists as the total rate of dissolution and residual trapping levels off between 2000 and 3000 years after injection ceases. These small plumes of CO_2 that remain in the "mobile" phase are evident in Figure 7, and they are created because the heterogeneity and caprock topography lead to a complex plume shape with mobile CO_2 trapped in local dome structures (as such, it is actually "immobile"). These small plumes do not dissolve and remain as a separate fluid phase because the surrounding

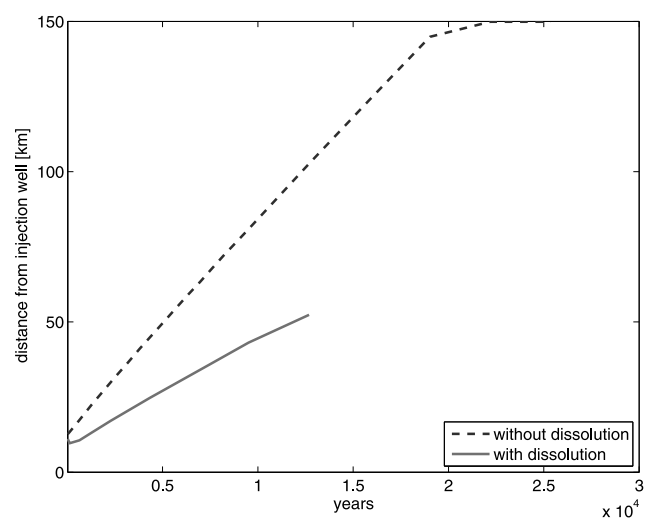

Figure 6. Comparison of maximum upslope extent measured as distance from the injection well over time for the benchmark problem. The solid line indicates the case with convection-enhanced dissolution, and the dashed line indicates the cases without dissolution.

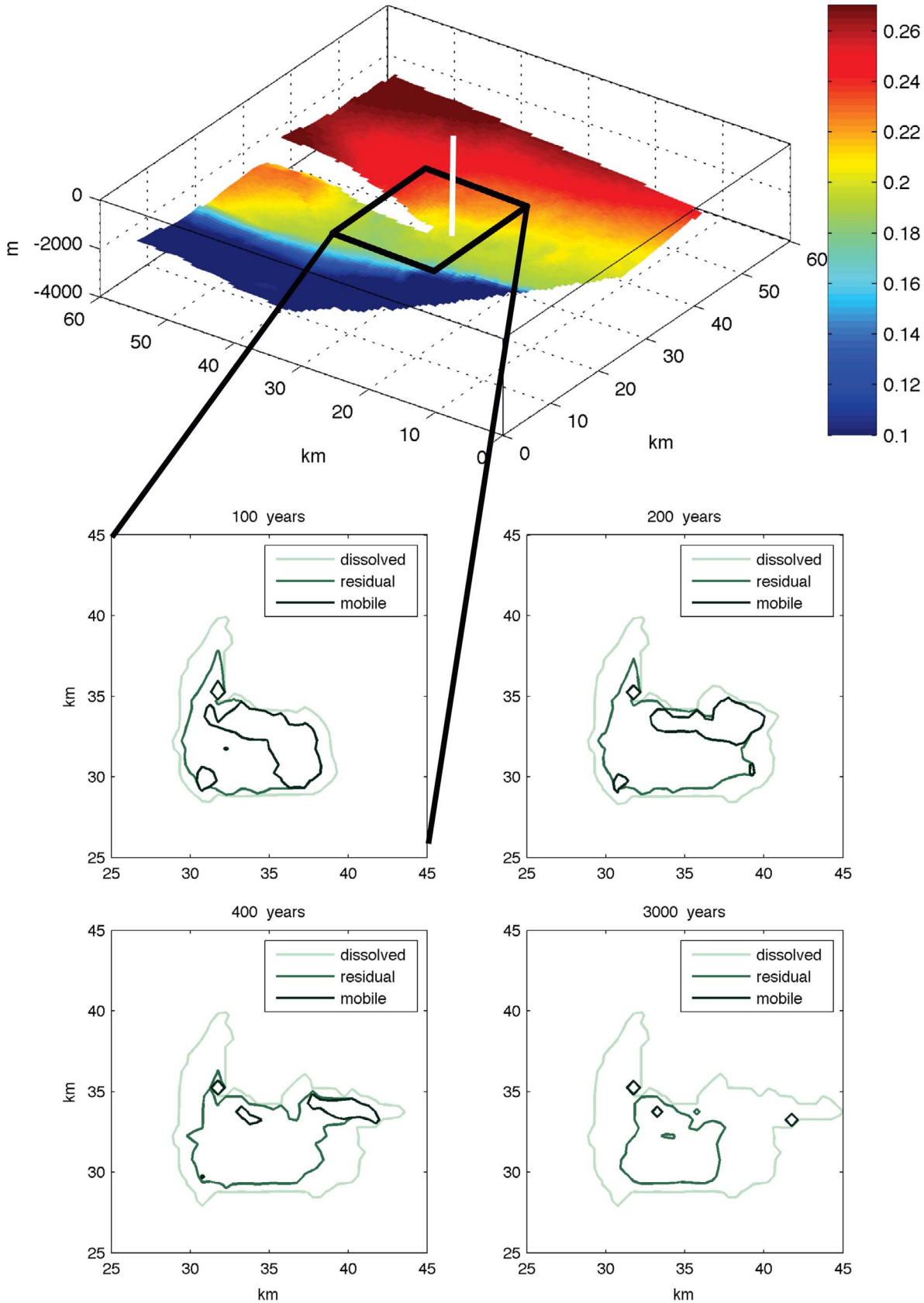

Figure 7. Numerical results of residual and solubility trapping in the Johansen formation during a 3000 year postinjection period. (top) The geological structure of the formation, indicating the injection well and the distribution of porosity. (bottom) Contour plots, indicating the outer edge of the different CO_2 regions (mobile, residual, and dissolved CO_2) within a subregion of the entire Johansen formation.

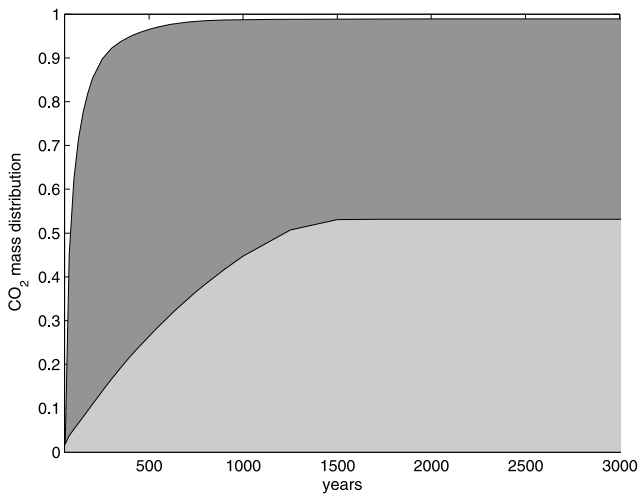

Figure 8. Distribution of CO_2 mass over time for the Johansen test problem with dissolution-convection effects included. The fraction of total CO_2 mass in the mobile phase is indicated by the white area, that in the residual phase by the dark gray area, and that in the dissolved phase by the light gray area.

brine is completely saturated with dissolved CO_2. In addition, the CO_2 bubbles do not continue to travel updip because they are trapped by the topography, thus effectively immobilizing the CO_2. This is an interesting result because structural trapping is typically thought of as an important mechanism in the injection and early postinjection periods. But we see now an instance where this type of trapping becomes somewhat important in the late postinjection period in cases where topographical features are more complex.

4. Summary and Discussion

[68] We have presented a vertically integrated sharp interface numerical model for CO_2 injection and long-term migration with residual and solubility trapping. Solubility trapping is modeled using an upscaled mass transfer model that has been derived within the vertically averaged framework. This upscaled mass transfer model captures local dissolution and convective mixing processes that occur below the scale of the grid block. To do this, two assumptions are made: (1) that the onset time of instability required for convection to begin is short compared to the timescale being modeled and (2) that once the onset time of instability has passed, the dissolution process is essentially linear and can be approximated by a constant rate of dissolution in time, up until the time that all of the brine below the macroscopic interface is saturated with CO_2. These assumptions have been shown in previous studies to be reasonable for typical deep geological systems. In this paper, we have shown that by simplifying a complex multiscale process, the effects of dissolution can be modeled over much larger spatial and temporal scales than would be possible using a traditional numerical model. Because the sharp interface model is solved numerically, this method is also a distinct improvement over analytical sharp interface models that are limited to ideal systems and have only been developed to date to include residual trapping in homogeneous formations.

[69] The model presented herein was applied to a simple benchmark problem to demonstrate the ability of the model to capture long-term trapping processes that are important for the stabilization of the CO_2 plume. We have also demonstrated that these processes can be modeled for very large, complex systems, such as the Johansen formation in the North Sea, over time periods on the order of 10,000 years. We have found that the addition of a dissolution-convection model in the benchmark problem greatly impacts long-term trapping of mobile CO_2 in two ways: (1) by reducing the maximum travel time by several thousand years and (2) by decreasing the maximum updip travel distance by 100 km or more. It should be noted that the benchmark results are not intended to be representative of real systems, and the time to stabilization and maximum distance traveled are measures that are very sensitive to system properties such as permeability. For many continental basins, the permeabilities are much lower than that used for this simple system, which implies much slower rates of migration in typical systems. In addition, we have found that for the Johansen formation, a more realistic geological system, the rates of migration are also affected by heterogeneity and structural complexity. This means that although the permeability of this system is generally high, the resulting rate of migration is relatively slow. Combined with convection-enhanced dissolution and residual trapping, the slow migration rate leads to complete immobilization after a few thousand years. The relatively long time to stabilization is countered by the fact that the plume never extends more than 15 km from the injection point. Therefore, it is important to consider the long-term immobilization of CO_2 as largely dependent on the properties of the system of interest.

[70] A sharp interface assumption was employed in the model development, which means we assume the capillary transition zone is small relative to the vertical length scale of the system. This implies that the model results for the benchmark and the Johansen cases do not include the effect of significant local capillary forces on long-term CO_2 migration. For systems where the capillary transition zone is a significant fraction of the aquifer height, local capillary effects will retard the upslope migration of the plume because of reduced local relative permeability values where local CO_2 saturation is small. This effect can be included within the vertically integrated framework by simply allowing both fluid phases to be mobile above the macroscopic interface ζ_M. The saturation profile is no longer constant in this region but is defined by the local capillary pressure function, with the integrated fluid fluxes accounting for the vertical variation in fluid mobility. The implementation of this model including capillary pressure effects will be the subject of future work.

[71] Simple, yet effective models such as the one presented herein are essential tools for understanding the long-term fate of sequestered CO_2 plumes at relevant spatial and temporal scales. The present model allows for insight into measures such as maximum travel distances and times before the CO_2 is effectively immobilized by capillary and solubility trapping mechanisms, without compromising the essential physics of the problem. These estimates can be obtained in a relatively short computational time frame, which would be impossible for standard high-resolution

numerical methods run on the most powerful computing architectures. As a result, this model may be of value to both operators and, especially, regulators. Although high-resolution numerical methods are still invaluable for examining the details of these complex, multiphysics, and multiscale processes, the utility of simple models is very important for assessing the long-term success of industrial-scale carbon capture and storage operations.

[72] **Acknowledgments.** Funding for S. E. Gasda is provided by a research fellowship through the King Abdullah University of Science and Technology (KAUST). This work was supported in part by the National Science Foundation under grant EAR-0934722, the Environmental Protection Agency under cooperative agreement RD-83438501, the Department of Energy under award DE-FE0001161, CFDA 81.089, and the Carbon Mitigation Initiative at Princeton University.

References

Bachu, S. (2002), Sequestration of CO_2 in geological media in response to climate change: Road map for site selection using the transform of the geological space into the CO_2 phase space, *Energy Convers. Manage.*, *43*, 87–102.

Barker, T., et al. (2007), Technical summary, in *Climate Change* 2007*: Mitigation. Contribution of Working Group III to the Fourth Assessment Report of the Intergovernmental Panel on Climate Change*, edited by B. Metz et al., pp. 25–93, Cambridge Univ. Press, Cambridge, U. K.

Bear, J. (1972), *Dynamics of Fluids in Porous Media*, Elsevier, New York.

Benson, S., et al. (2005), Underground geological storage, in *Carbon Dioxide Capture and Storage, Intergovernmental Panel on Climate Change Special Report*, edited by B. Metz et al., pp. 95–276, Cambridge Univ. Press, New York.

Celia, M. A., and J. M. Nordbotten (2009), Practical modeling approaches for geological storage of carbon dioxide, *Ground Water*, *47*(5), 627–638.

Class, H., et al. (2009), A benchmark study on problems related to CO_2 storage in geologic formations, *Comput. Geosci.*, *13*(4), 409–434.

Coats, K., J. Dempsey, and J. Henderson (1971), Use of vertical equilibrium in 2-dimensional simulation of 3-dimensional reservoir performance, *Soc. Pet. Eng. J.*, *11*(1), 63–71.

Dentz, M., and D. T. Tartakovsky (2009a), Abrupt-interface solution for carbon dioxide injection into porous media, *Transp. Porous Media*, *79*, 15–27.

Dentz, M., and D. T. Tartakovsky (2009b), Response to "Comments on abrupt-interface solution for carbon dioxide injection into porous media by Dentz and Tartakovsky (2008)" by Lu et al., *Transp. Porous Media*, *79*, 39–41.

Dietz, D. L. (1953), A theoretical approach to the problem of encroaching and by-passing edge water, in *Proc. K. Ned. Akad. Wet., Ser. B Phys. Sci.*, *56*, 83–92.

Eigestad, G. T., H. K. Dahle, B. Hellevang, F. Riis, W. T. Johansen, and E. Øian (2009), Geological modeling and simulation of CO_2 injection in the Johansen formation, *Comput. Geosci.*, *13*(4), 435–450.

Ennis-King, J., and L. Paterson (2005), Role of convective mixing in the long-term storage of carbon dioxide in deep saline formations, *SPE J.*, *10*(3), 349–356.

Farajzadeh, R., H. Salimi, L. J. P. Zitha, and H. Bruining (2007), Numerical simulation of density-driven natural convection in porous media with application for CO_2 injection projects, *Int. J. Heat Mass Transfer*, *50*(25-26), 5054–5064.

Freeze, R., and J. Cherry (1979), *Groundwater*, Prentice-Hall, Englewood Cliffs, N. J.

Gasda, S. E., S. Bachu, and M. A. Celia (2004), Spatial characterization of the location of potentially leaky wells penetrating a deep saline aquifer in a mature sedimentary basin, *Environ. Geol.*, *46*(6-7), 707–720.

Gasda, S. E., J. M. Nordbotten, and M. A. Celia (2009), Vertical equilibrium with sub-scale analytical methods for geological CO_2 sequestration, *Comput. Geosci.*, *13*(4), 435–450.

Hesse, M. A., F. M. Orr Jr., and H. A. Tchelepi (2008), Gravity currents with residual trapping, *J. Fluid Mech.*, *611*, 35–60.

Holloway, S. (2005), Underground sequestration of carbon dioxide—A viable greenhouse gas mitigation option, *Energy*, *30*(11-12), 2318–2333.

Huppert, H., and A. Woods (1995), Gravity-driven flows in porous layers, *J. Fluid Mech.*, *292*, 55–69.

Juanes, R., C. W. MacMinn, and M. L. Szulczewski (2010), The footprint of the CO_2 plume during carbon dioxide storage in saline aquifers: Storage efficiency for capillary trapping at the basin scale, *Transp. Porous Media*, *82*, 19–30.

Lake, L. (1989), *Enhanced Oil Recovery*, Prentice-Hall, Upper Saddle River, N. J.

Lindeberg, E., and D. Wessel-Berg (1997), Vertical convection in an aquifer column under a gas cap of CO_2, *Energy Convers. Manage.*, *38*, Suppl. S, S229–S234.

Lindeberg, E., P. Bergmo, and A. Moen (2003), The long-term fate of CO_2 injected into an aquifer, in *Proceedings of the 6th International Conference on Greenhouse Gas Control Technologies*, edited by J. Gale and Y. Kaya, pp. 489–494, Pergamon, Amsterdam.

Lyle, S., H. Huppert, M. Hallworth, M. Bickle, and A. Chadwick (2005), Axisymmetric gravity currents in a porous medium, *J. Fluid Mech.*, *543*, 293–302.

Lu, C., S. Lee, W. S. Han, B. J. McPherson, and P. C. Lichtner (2009), Comments on "Abrupt-interface solution for carbon dioxide injection into porous media" by M. Dentz and D. Tartakovsky, *Transp. Porous Media*, *79*, 29–37.

Neufeld, J. A., and H. E. Huppert (2009), Modelling carbon dioxide sequestration in layered strata, *J. Fluid Mech.*, *625*, 353–370.

Nordbotten, J. M., and M. A. Celia (2006), Similarity solutions for fluid injection into confined aquifers, *J. Fluid Mech.*, *561*, 307–327.

Nordbotten, J. M., and M. A. Celia (2009), Practical modeling approaches for geological storage of carbon dioxide, *Ground Water*, *47*(5), 627–638.

Nordbotten, J. M., and H. K. Dahle (2011), Impact of the capillary fringe in vertically integrated models for CO_2 storage, *Water Resour. Res.*, *47*, W02537, doi:10.1029/2009WR008958.

Pacala, S., and R. Socolow (2004), Stabilization wedges: Solving the climate problem for the next 50 years with current technologies, *Science*, *305*, 968–972.

Pruess, K. (2008), Numerical modeling studies of the dissolution-diffusion-convection process during CO_2 storage in saline aquifers, *Tech. Rep. LBNL*-1243*E*, Lawrence Berkeley Natl. Lab., Berkeley, Calif.

Riaz, A., M. Hesse, H. A. Tchelepi, and F. M. Orr (2006), Onset of convection in a gravitationally unstable diffusive boundary layer in porous media, *J. Fluid Mech.*, *548*, 87–111.

Vella, D., and H. Huppert (2006), Gravity currents in a porous medium at an inclined plane, *J. Fluid Mech.*, *555*, 353–362.

Yortsos, Y. C. (1995) A theoretical analysis of vertical flow equilibrium, *Transp. Porous Media*, *18*, 107–129.

M. A. Celia, Department of Civil and Environmental Engineering, Princeton University, Engineering Quadrangle, Princeton, NJ 08544, USA.

S. E. Gasda, Environmental Sciences and Engineering, University of North Carolina at Chapel Hill, 148 Rosenau Hall, Chapel Hill, NC 27599, USA. (sgasda@unc.edu)

J. M. Nordbotten, Department of Mathematics, University of Bergen, NO-5020 Bergen, Norway.